The Structures of Small Platinum Cluster Anions Pt_n^-: Experiment and Theory

Dennis Bumüller,[†] Asfaw G. Yohannes,[*,†,‡] Stephan Kohaut,[†] Ivan Kondov,[‡] Manfred M. Kappes,[¶,†] Karin Fink,[†] and Detlef Schooss[*,†]

†*Institute of Nanotechnology, Karlsruhe Institute of Technology (KIT), Hermann-von-Helmholtz-Platz 1, 76344 Eggenstein-Leopoldshafen, Germany*

‡*Steinbuch Centre for Computing, Karlsruhe Institute of Technology (KIT), Hermann-von-Helmholtz-Platz 1, 76344 Eggenstein-Leopoldshafen, Germany*

¶*Institute of Physical Chemistry, Karlsruhe Institute of Technology, Fritz-Haber-Weg 2, 76131 Karlsruhe, Germany*

E-mail: asfaw.yohannes@ucalgary.ca; detlef.schooss@kit.edu

Abstract

The structures of platinum cluster anions Pt_6^- - Pt_{13}^- have been investigated by trapped ion electron diffraction. Structures were assigned by comparing experimental and simulated scattering functions using candidate structures obtained by density functional theory computations, including spin-orbit coupling. We find a structural evolution from planar structures (Pt_6^-, Pt_7^-) and amorphous-like structures (Pt_7^- - Pt_9^-) to structures based on distorted tetrahedra (Pt_9^- - Pt_{11}^-). Finally, Pt_{12}^- and Pt_{13}^- are based on hcp fragments. While the structural parameters are well described by density functional theory computations for all clusters studied, the predicted lowest energy structure is found in the experiment only for Pt_6^-. For larger clusters higher energy isomers are necessary to obtain a fit to the scattering data.

Introduction

Platinum is used as versatile catalyst and utilized in technical applications for a wide variety of reactions. It is used for example as catalyst in automotive catalytic converters, in the oxygen reduction reaction,[1,2] in the hydrogen evolution reaction[3] or in dehydrogenation reactions of hydrocarbons.[4] For economic reasons, a reduction of the necessary amount of platinum is of great interest. In this context, it was found that small platinum clusters show high catalytic activity in various reactions, in most cases strongly size dependent.[5–11] For example, Heiz *et al.* found a distinct cluster size dependence for the CO-oxidation on MgO.[5] Vajda *et al.*[6] reported that the catalytic activity of supported Pt_8-Pt_{10} clusters is 40-100 times higher than for vanadia based catalysts in the oxidative dehydrogenation of propane and Imaoka *et al.*[7,8] inferred that the catalytic activity of Pt_{12} is twice as high as for Pt_{13}.

The study of platinum clusters in the gas phase supported by advanced theoretical methods offers a route to model such catalytic systems and can contribute towards clarifying the mechanisms of the reaction processes. An important prerequisite for the latter is, however, the knowledge of the cluster structure.

Direct or indirect experimental information on the geometrical structure of small platinum clusters is hardly available. Lineberger *et al.* determined the photo-electron spectrum of Pt_3^- and Fielicke *et al.* used infra-red multiphoton dissociation spectroscopy to study the structures of $Pt_{3\text{-}5}{}^+$.[12] Very recently, Henninen *et al.* showed by using scanning transmission electron microscopy that small Pt clusters on graphite can have fcc geometries at elevated temperatures.[13]

There are some theoretical studies on small Pt clusters, but mostly restricted to neutral clusters[14–20]. However, for small clusters the structure can be charge dependent.[21,22] In case of platinum clusters, only Chaves et al.[23] computed structures for $Pt_{2\text{-}14}{}^{-/0/+}$ and indeed found distinct global minimum structures for different charge states.

Overall, the computational studies on platinum clusters are rather inconclusive with respect to the lowest energy structure. For example, Kumar et al.[16] proposed planar structures up to Pt_9, while Demiroglu et al.[18] found 3D motifs starting with Pt_7. In addition, small Pt_n clusters show a high structural diversity,[17,24] that is a high number of isomers in a small energy range. While this property is important to explain the high catalytic activity[25] it hampers the prediction of the global minimum structure. Considering a typical error of density functional (DFT) computations, a clear assignment is often not possible. Additionally, the accurate prediction of ground state of heavy elements, such as Pt, requires taking the computationally more demanding spin-orbit coupling (SOC) into account.[26,27] In particular, SOC has been found to have a significant effect on the relative stability of isomers.[28–30] In summary, these uncertainties require a validation of the structural predictions by experimental means.

We are not aware of any experimental study on the structures of Pt_n^- (n>5). The aim of this work is therefore to establish the equilibrium structures of platinum cluster anions in a range from $n = 6 - 13$ via a combination of trapped ion electron diffraction (TIED) and DFT computations. We chose anionic clusters, because TIED has a higher sensitivity for negatively charged ions than for cations.[31] The smallest Pt-cluster in this study ($Pt_6{}^-$) is at

the lower limit of the TIED experiment, whose signal-to-noise ratio increases with cluster nuclearity. Structures are assigned based on comparison of experimental and simulated scattering functions from candidate structures, which are obtained by computational methods. Such a synergistic approach has been applied successfully in a number of studies for other metal clusters[22,32,33] and allows in most cases for an unequivocal structural assignment.

Methods

Trapped Ion Electron Diffraction

The TIED experiment has been described in detail elsewhere.[31,34] Platinum cluster anions were generated by a magnetron sputter source,[35] mass selected to a single cluster size and trapped in a quadrupole ion trap held at about 95 K. Thermal equilibrium of the anions was achieved by collisions with He buffer gas at a pressure of 0.01 mbar for several seconds. A 40 keV electron beam crossed the ion cloud, consisting of 10^5-10^6 cluster ions. Electrons scattered during an exposure time of 20-30 s were detected by a phosphor screen and integrated on an external CCD camera. For a total measurement, about 100 – 2000 of background-corrected diffraction pictures have been accumulated and averaged – depending on cluster size and corresponding ion intensity. The total scattering intensity $I_{\mathrm{tot}}^{\mathrm{exp}}$ as function of the electron momentum transfer $s = \frac{4\pi}{\lambda} \sin \frac{\theta}{2}$ with the electron wavelength λ and the scattering angle θ was extracted by radially averaging the sum of the background corrected diffraction pictures. Using the atomic scattering intensity I_{at}[36] and an additional unspecific polynomial based background I_{back}, the experimental reduced molecular scattering intensity $sM^{\mathrm{exp}}(s) = s(I_{\mathrm{tot}} - I_{\mathrm{at}} - I_{\mathrm{back}})/I_{\mathrm{at}}$ was calculated. In order to compare these results with candidate structures, the theoretical reduced molecular scattering function was approximated by

$$sM^{\mathrm{theo}}(s) = \frac{S_{\mathrm{c}}}{N} \exp\left(-\frac{L^2}{2} s^2 \right) \sum_{i}^{N} \sum_{j \neq i}^{N} \frac{\sin(s k_{\mathrm{s}} r_{ij})}{k_{\mathrm{s}} r_{ij}} \qquad (1)$$

where N is the number of atoms in the cluster, r_{ij} the inter-atomic distances, and L an averaged mean vibrational amplitude. S_c and k_s are scaling factors for the amplitudes and the distances. Experimental broadening is considered by convolution of sM^{theo} with a Gaussian ($\sigma = 0.15$ $\mathring{A}^{-1}$) and attenuation by the finite trap opening by weighting with an error-function centered at the maximum angle ($s = 14$ $\mathring{A}^{-1}$). For comparison of theoretical and experimental data a χ^2-fit minimizing the weighted differences by variation of S_{c}, k_{s}, L and the parameters of I_{back} was performed.

We use the weighted profile factor $R_{\mathrm{w}} = \sqrt{\sum_i w_i (sM_i^{\mathrm{theo}} - sM_i^{\mathrm{exp}})^2 / \sum_i w_i (sM_i^{\mathrm{exp}})^2}$ to characterize the degree of agreement of candidate structure and experimental data.[34] The weights w_i were calculated from the error propagated standard deviation of the experimental data.

Density Functional Theory Computations

Structural models for TIED fitting were obtained from a combination of different methods. Semi-empirical potentials (Gupta[37,38] or Morse[39]) were used within a modified genetic algorithm (GA) to generate experimentally well fitting candidate structures.[40,41] These were further optimized using DFT computations with the TURBOMOLE package.[42] In addition, extensive global minimum searches were performed using a DFT based GA.[43] A population size of 30 structures with 10 children has been employed. The calculations were carried out until no new minimum structures were found within 45 generations. Typically, the putative global minimum structures have been obtained in less than 35 generations. For the local structure optimization, a split valence polarization (def2-SVP) basis set[44] and the BP86 functional[45] were employed. The RI-J (resolution of the identity for the Coulomb term J) approximation[46,47] as well as effective core potentials (ECP) (1s-4f in core)[48], which account for scalar relativistic effects, have been used throughout. Pt_n^- clusters are open shell systems (odd number of electrons) and can occur in different spin states. Therefore, the GA calculations were performed for different numbers of unpaired electrons using the unrestricted

Kohn-Sham method.

The geometries of 10-20 isomers with low energies and/or small profile factors have been reoptimized with the TPSS[49] functional in combination with a def2-TZVP basis set.[44,48] We have chosen the TPSS/def2-TZVP method because it leads to a better description of the structural parameters, for example bond distances, determined from the comparison of simulated and experimental scattering function. Furthermore, TPSS has been successfully used on Bi_n^+ [27] and Au_n^- [50]. The lowest-energy electronic state was obtained by applying a Fermi smearing to allow fractional occupations with an initial temperature T = 600 K, which was progressively lowered during the self-consistent field iterations down to T = 50 K. By starting the calculation with high numbers of unpaired electrons usually integer occupations and electronic states without holes were achieved. If not mentioned otherwise, all structure optimizations have been carried out without symmetry restrictions. The symmetries of the final optimized structures were determined using the TURBOMOLE *desy* command. The resulting point groups were analyzed, and vibrational frequency calculations were performed to confirm that the final structures are local minima. The coordinates of all structures shown here are given in the supporting information (SI).

Finally, the relative energies for the different isomers at each cluster size were recalculated, considering different further contributions. SOC was included by relativistic two-component (2C) calculations[51] with the TPSS functional and the dhf-TZVP-2c basis set.[52,53] SOC often has a significant influence on the relative energies of different isomers. It has to be mentioned that we did not re-optimize the structures with inclusion of SOC which could slightly change the structures as has been observed for Bi_n^+ clusters.[27] Furthermore, the effect of dispersion corrections was evaluated using DFT-D3 with Becke-Johnson damping.[54] Finally, thermal corrections to the DFT energy are included by computing the Gibbs free energy (ΔG) at 95 K and 1 bar.

Results

In the following, we compare candidate structures from DFT computations to the experimental TIED data. On the order 10-15 cluster structures have been finally analyzed for each cluster size. Here only the most relevant are described, that are the lowest energy structures or the ones that fit best to the experimental data. Table 1 summarizes our results. It shows for each size and isomer the relative energy using TPSS/def2-TVZP and the relative energy including SOC from single point calculations using 2C-TPSS/dhf-TZVP-2c computations, the ground state multiplicity, the point group, and the corresponding experimental profile factor R_W. Dispersion corrections did not affect the relative energies significantly and the ordering remains the same as for TPSS/def2-TZVP. Similarly, the consideration of the experimental temperature did not lead to change in the relative (free) energy ordering. We summarize the latter results in the supporting information (Table S1).

Pt_6^-

Fig.1 shows the lowest energy structures for Pt_6^- using TPSS/def2-TZVP. The predicted lowest energy isomer (1) is in agreement with Ref. 23 and several calculations on neutral Pt_6.[14–16,18,19] It is a planar D_{3h} structure with triangular shape. The 3D isomer (2) is 0.11 eV higher in energy. For a depiction of the non-planar distortions, please see Fig. S1. Finally, the planar rectangular isomer (3) is at 0.30 eV. The SOC increases the relative difference, but has no effect on the energetic ordering of the isomers.

The comparison of measured and calculated scattering functions shown in Fig. 2 fully supports the computations. The theoretical scattering function of structure (1) matches the experimental data very well ($R_{\mathrm{w}} = 1.7\%$) while other isomers can be ruled out.

Pt_7^-

A subset of structures for Pt_7^- considered in this work is shown in Fig. 3. The lowest energy isomer within TPSS/def2-TZVP is a triangular structure with a split cap (1). It can be

Table 1: Relative energies ΔE for Pt_n^- clusters at the TPSS/def2-TZVP and 2C-TPSS/dhf-TZVP-2c level together with point group P, multiplicity M and profile factor R_w. The isomers found in the experiment are highlighted in bold.

Cluster	$\Delta E/eV$	$\Delta E_{2C}/eV$	P	M	$R_w/\%$
Pt_6^-(1)	0.00	0.00	D_{3h}	2	1.7
Pt_6^-(2)	0.11	0.22	C_{2v}	2	7.8
Pt_6^-(3)	0.30	0.44	D_{2h}	2	10.3
Pt_7^-(1)	0.00	0.02	C_{2v}	6	8.2
Pt_7^-(2)	0.21	0.03	D_{3d}	2	6.5
Pt_7^-(3)	0.21	0.09	C_1	6	13
Pt_7^-(4)	0.22	0.00	C_2	2	18
Pt_7^-(5)	0.35	0.01	C_2	2	4.2
Pt_7^-(6)	0.90	0.67	C_s	2	2.6
Pt_8^-(1)	0.00	0.08	C_s	2	27
Pt_8^-(2)	0.03	0.00	C_s	4	8.4
Pt_8^-(3)	0.27	0.13	C_s	2	7.9
Pt_8^-(4)	0.32	0.25	C_1	4	4.8
Pt_8^-(5)	0.33	0.33	C_2	2	13
Pt_8^-(6)	0.56	0.35	C_1	4	2.0
Pt_9^-(1)	0.00	0.05	C_s	2	18
Pt_9^-(2)	0.15	0.02	C_2	2	6.7
Pt_9^-(3)	0.16	0.00	C_1	2	9.8
Pt_9^-(4)	0.41[a]	0.01	C_s	2	4.8
Pt_{10}^-(1)	0.00	0.00	T_d	8	5.6
Pt_{10}^-(2)	0.11	0.14	C_s	6	3.5
Pt_{10}^-(3)	0.21	0.28	C_2	2	5.4
Pt_{11}^-(1)	0.00	0.00	C_2	2	19
Pt_{11}^-(2)	0.07	0.14	C_1	2	12
Pt_{11}^-(3)	0.32	0.16	C_s	2	2.9
Pt_{12}^-(1)	0.00	0.00	C_1	2	26
Pt_{12}^-(2)	0.35	0.25	C_1	2	6.8
Pt_{12}^-(3)	0.63	0.18	C_{2v}	2	3.0
Pt_{13}^-(1)	0.00	0.00	C_s	2	26
Pt_{13}^-(2)	0.36	0.32	C_1	2	11
Pt_{13}^-(3)	0.61	0.14	C_{3v}	2	4.1

[a] saddle point

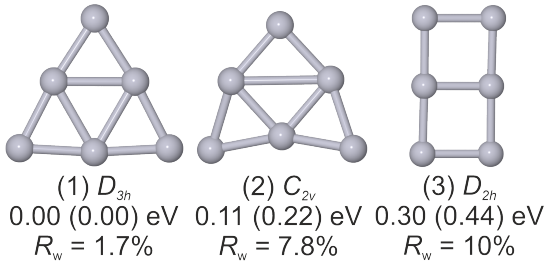

Figure 1: Lowest energy isomers of Pt_6^- with point group, relative energy for TPSS/def2-TZVP , the SOC corrected value (in parentheses) and the experimental profile factor.

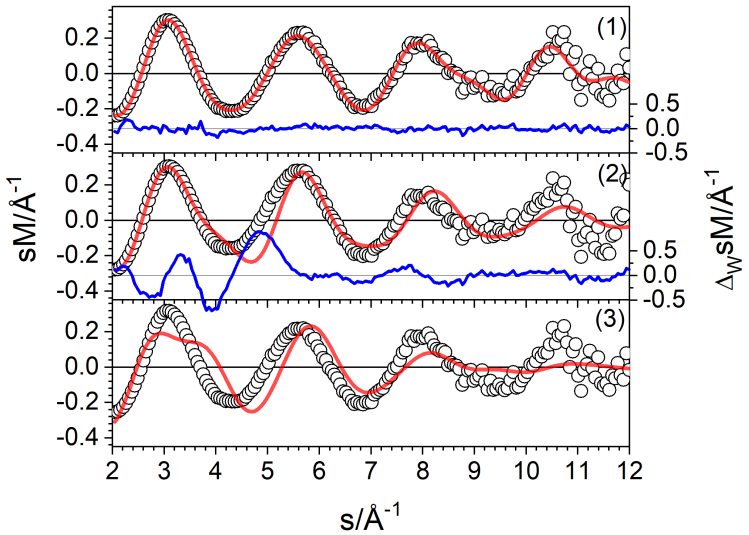

Figure 2: Comparison of experimental (circles) and simulated (red line) modified molecular scattering intensities sM for isomers (1)-(3) of Pt_6^-. The blue lines in panel (1) and (2) show the weighted residuals.

obtained from Pt_6^--(1) by replacing one of the apex atoms by a dimer perpendicular to the triangular plane. Structure (2) is a non-planar distorted hexagon with D_{3d} symmetry at 0.21 eV, isoenergetic with structure (3), which can be seen as two face-connected (distorted) quadratic pyramids. Isomer (4) at 0.22 eV is a planar side-capped ladder and was found as the lowest in energy in the calculations of Chaves et al.[23] The replacement of one of the edge atoms of the Pt_6^--(1) with a dimer perpendicular to the triangular plane leads to isomer (5) at 0.35 eV. The inclusion of SOC calculation on top of TPSS/def2-TZVP has a significant influence on the energy ordering of the isomers: now isomers (1)-(5) have virtually the same energy.

None of the structures (1)-(5) lead to a satisfactory agreement with the experimental data (see Table 1 and Fig. 4). A low R_w is obtained only for the high lying (0.90 eV) C_s isomer (6). It can be seen as two distorted tetrahedra sharing a common atom. Forcing this structure into C_{2v} symmetry increases the relative energy as well as the R_w value significantly (not shown). However, if we allow for two component combinations among the low-lying isomers (1-5) a similarly good agreement with the TIED data can be obtained. In particular, a mixture of isomer (2, 59%) with (3) shows a low profile factor of $R_{\mathrm{w}} = 2.7\%$ (Fig. 4).

Pt_7^- turns out to be an unusual case, as we have found five isomers within 0.1 eV. Additionally, the TIED data does not lead to unique assignment, if considering only single isomer or two component mixtures describing the experimental composition. However, taking into account the high energy of isomer (6) even under considerations of SOC, we tentatively assign Pt_7^- to a mixture of structures consisting mainly of the quasi-planar (2) and the 3D structure (3) under the experimental conditions. However, small contributions ($< 5\%$) from other isomers in a multi-component mixture cannot be ruled out.

Pt_8^-

A set of low energy isomers for Pt_8^- is shown in Fig. 5. The blue putative global minimum within TPSS/def2-TZVP is the so called gyrobifastigium (1) and can be constructed by

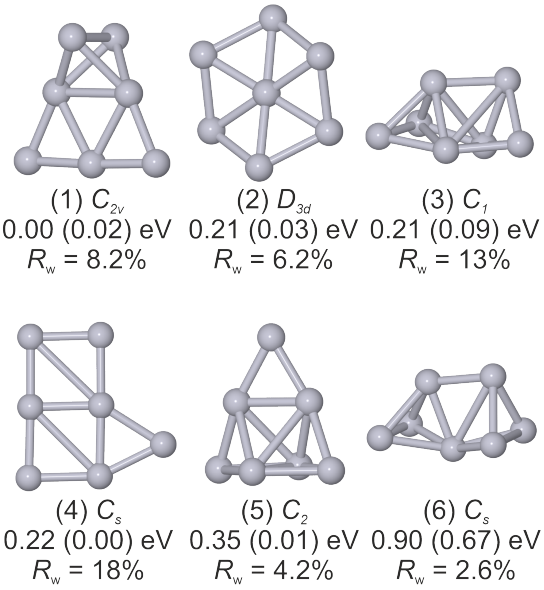

Figure 3: Pt_7^- isomers with point group, relative energy for TPSS/def2-TZVP, the SOC corrected value (in parentheses) and experimental profile factor.

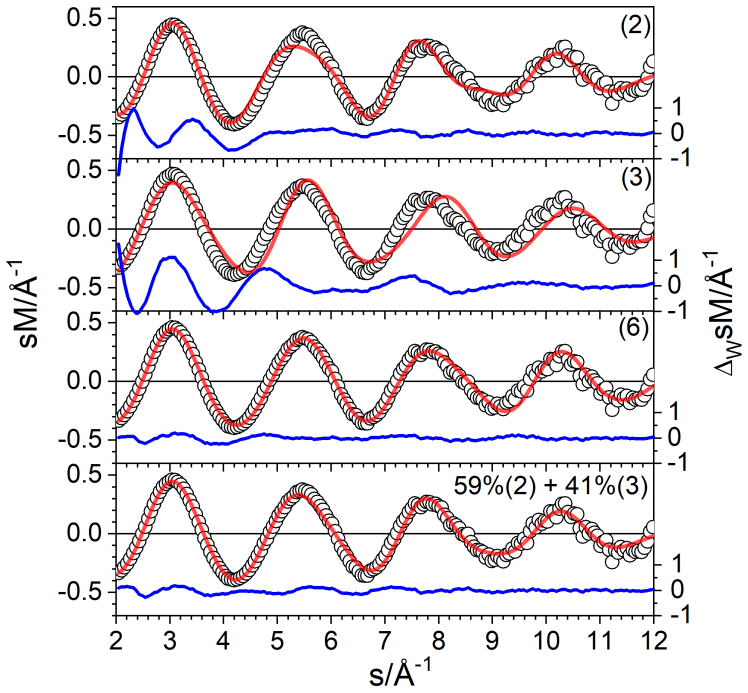

Figure 4: Comparison of experimental (grey circles) and simulated (red line) modified molecular scattering intensities sM for isomers (2), (3), (6) and for a mixture of isomers (2) and (3) of Pt_7^-. The blue line in each panel shows the weighted residuals.

joining two face-regular triangular prisms. Structure (2) is a triple capped (distorted) square pyramid and is quasi-isoenergtic (0.03 eV) with structure (1). Structures (3) and (4) consist of face and edge capped connected trigonal pyramids. Their energies are at 0.27 and 0.32 eV, respectively. Structure (4) (0.32 eV) is a quasi planar isomer based on the ladder structure (3) of Pt_6^- and was found as lowest energy structure for Pt_8^- in Ref. 23. Finally, isomer (6) at 0.56 eV consists of connected trigonal and square pyramids. Considering of SOC inverts the energy difference between isomer (1) and (2) and reduces the difference for most of the other isomers.

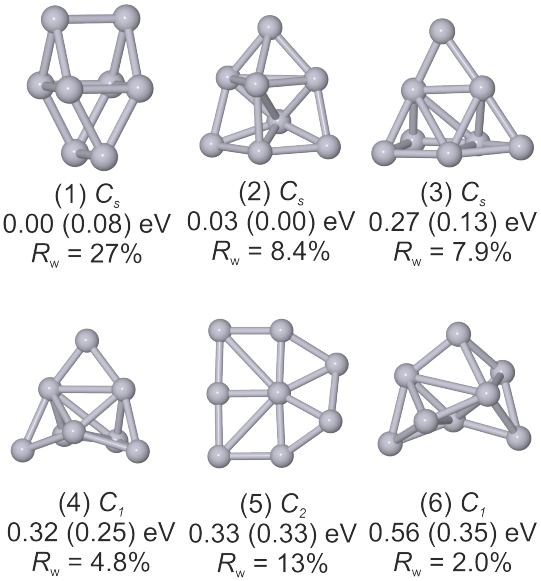

Figure 5: Pt_8^- isomers with point group, relative energy for TPSS/def2-TZVP, the SOC corrected value (in parentheses) and experimental profile factor.

Fig.6 shows the comparison of simulated and experimental scattering functions for Pt_8^-. Most structures shown here can be ruled out based on a high profile factor (1-3,5). The best agreement with the experimental data is found for isomer (6) with an profile factor of $R_w = 2.0\%$, significantly lower than isomer (4) with $R_w = 4.8\%$. Two component mixtures do not reduce the profile factor here and we conclude that even though isomer (6) is the highest energy isomer in the considered set, it represents the most probable contributor to the scattering experiment.

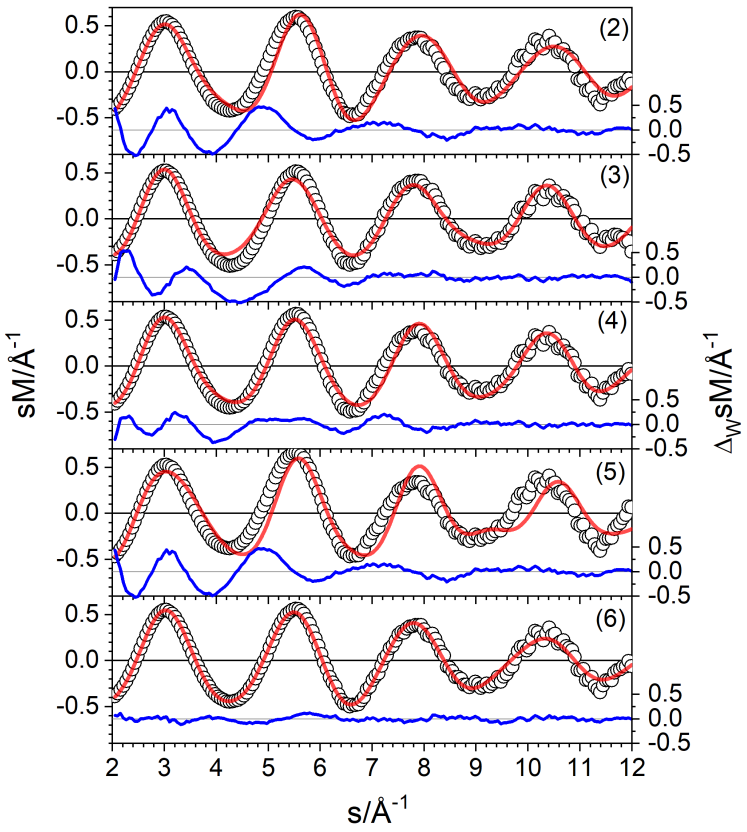

Figure 6: Comparison of experimental (grey circles) and simulated (red line) modified molecular scattering intensities sM for isomers (2)-(6) of Pt_8^-. The blue line in each panel shows the weighted residuals.

Pt_9^-

Four isomers of Pt_9^- are shown in Fig. 7. The putative global minimum at the TPSS/def2-TZVP level, isomer (1), has C_s symmetry and is a capped gyrobifastigium. Structure (2) at 0.15 eV is a tricapped triangular prism, and structure (3) at 0.16 eV can be described as a distorted version of isomer (2). Finally, at 0.41 eV a truncated tetrahedron is found having C_{3v} symmetry. It turns out that within TPSS/def2-TZVP this structure is a saddle point with imaginary frequencies of e and a_2-character. The lowest energy was obtained with a spin multiplicity of 8 and a singly occupied e-orbital causing Jahn-Teller distortion. However, after inclusion of SOC, isomer (4) is a true minimum structure as proved by a vibrational frequency calculation. The structural parameters insignificantly deviate from the TPSS/def2-TZVP structure and the energy difference to the single point value is negligible (0.01 eV). Overall the 2C computations have a strong impact on the relative energies, as all isomers are now quasi-isoenergetic.

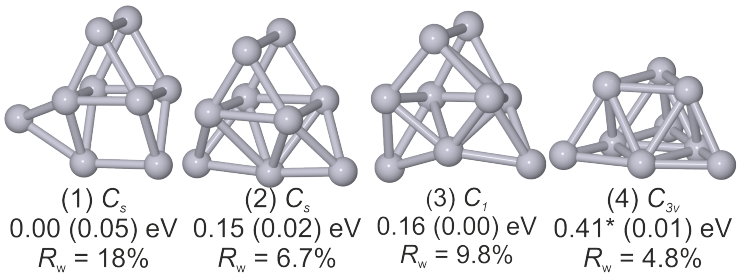

Figure 7: Pt_9^- isomers with point group, relative energy for TPSS/def2-TZVP, the SOC corrected value (in parentheses) and experimental profile factor. Isomer (4) is a minimum structure only in the 2C computation. Within TPSS/def2-TZVP the energy is given for the C_{3v} restricted configuration.

A planar D_{4h} isomer (not shown) found by Chaves et al.[23] is at 0.34 eV (TPSS/def2-TZVP) but can be clearly ruled out on basis of the TIED data. Among the structures shown here, only isomer (4) shows a reasonable agreement $R_w = 4.8\%$ with the experimental data. The weighted difference however shows still significant deviations with an oscillation pattern similar to the scattering function itself, which is an indication that a second motif is missing.

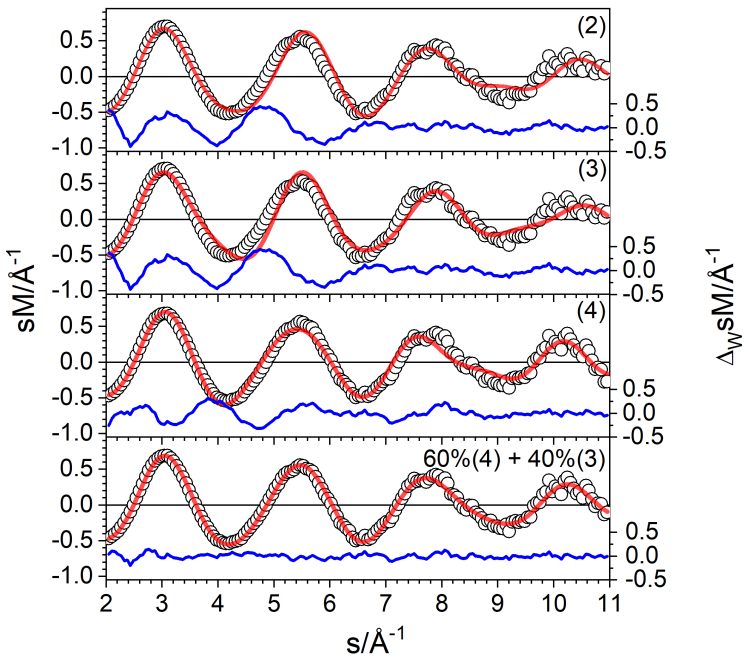

Figure 8: Comparison of experimental (grey circles) and simulated (red line) modified molecular scattering intensities sM for isomers (2)-(4) and a mixture of isomers (3) and (4) of Pt_9^-. The blue line in each panel shows the weighted residuals.

And indeed, this is the case here as shown in Fig. 8: including isomer (3) with $\approx$ 40% in a two component fit leads to a significant reduction of the profile factor ($R_w = 0.19\%$). Accordingly, we assign Pt_9^- to a mixture of a truncated tetrahedron and a distorted triangular prism.

$\mathbf{Pt_{10}^-}$

A subset of structures for Pt_{10}^- is shown in Fig. 9. In agreement with the results of Chaves et al., the global minimum (1) for Pt_{10}^- is a tetrahedron (T_d) with seven unpaired electrons representing a cutout from the fcc bulk structure. The same structural motif was also obtained for neutral and positively charged Pt_{10}.[23] Tetrahedral like structures (2) and (3) are found at 0.11 eV and 0.21 eV and have an increasing degree of distortion while at the same time their multiplicity is reduced. 2C computations do not change the energetic order of the isomers.

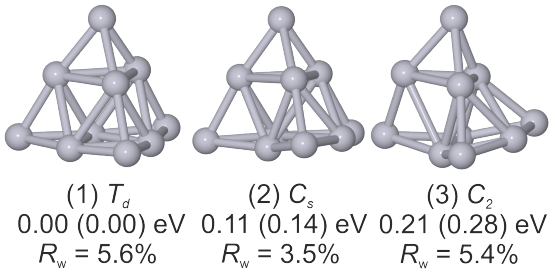

Figure 9: Pt_{10}^- isomers with point group, relative energy for TPSS/def2-TZVP, the SOC corrected value (in parentheses) and experimental profile factor.

Fig.10 shows the comparison of experimental and simulated scattering functions. The best agreement to the TIED data is obtained for the distorted tetrahedral geometry (2) with R_w value of 3.6 % in C_s symmetry. Other structures, including the predicted tetrahedral ground-state, have significantly higher profile factors. Mixtures among these isomers do not lead to a reduction of the profile factor. Accordingly, we assign structure (2) for Pt_{10}^-.

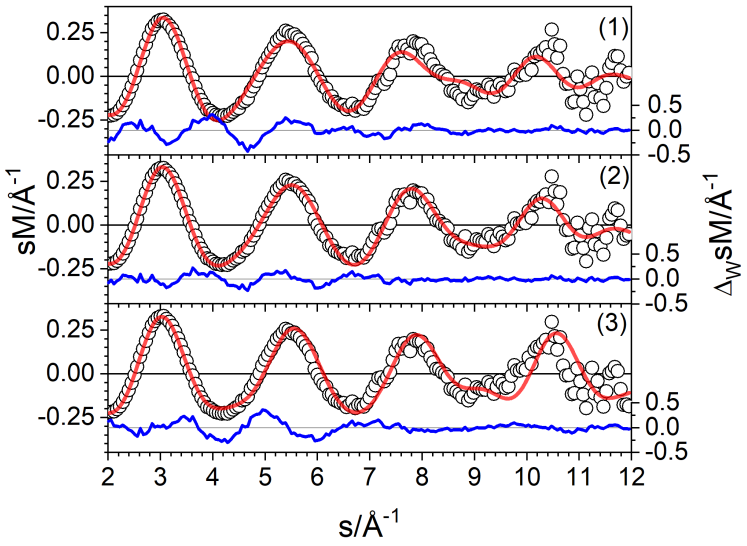

Figure 10: Comparison of experimental (grey circles) and simulated (red line) modified molecular scattering intensities sM for isomers (1)-(3) of Pt_{10}^-. The blue line in each panel shows the weighted residuals.

Pt_{11}^-

The most relevant structures for Pt_{11}^- are shown in Fig. 11. The predicted lowest energy isomer (1) has a tetrahedral shape, but is not a capped version of one of the isomers shown for Pt_{10}^-. Almost iso-energetic (0.07 eV) is structure (2), a capped version of structure (2) of Pt_{10}^-. Finally, isomer (3) at 0.32 eV is the capped T_d isomer of Pt_{10}^-. Including SOC does not change the energetic order.

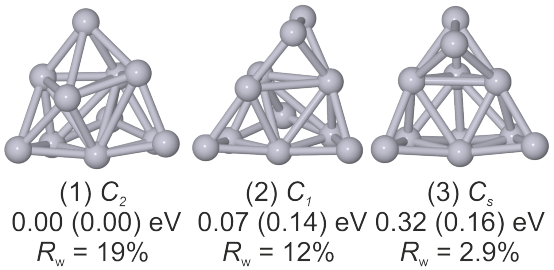

Figure 11: Pt_{11}^- isomers with point group, relative energy for TPSS/def2-TZVP, the SOC corrected value (in parentheses) and experimental profile factor.

Neither structure (1) nor structure (2) are able to explain the experimental scattering function (Fig. 12). Only the capped T_d structure (3) fits well to the experimental data with an R_w value of 2.9 %.

Pt_{12}^-

The putative global minimum (1) for Pt_{12}^- is a capped double layered triangular structure (Fig. 13). The simulated diffraction pattern, however, is not able to fit the TIED data as shown in Fig. 14. A better fit is found for the bi-capped tetrahedral isomer (2) at 0.35 eV (0.25 eV SOC). Finally, the best fitting structure ($R_w = 3.0\%$) is isomer (3), a doubly truncated trigonal bipyramid. It has a ABA layer structure and can be seen as a cutout of the hcp lattice. Its relative energy within TPSS/def2-TZVP is 0.63 eV, however, when using 2C computations it is reduced to 0.18 eV. If mixed with isomer (2)(38%) the profile factor reduces further to $R_w = 2.1\%$ (see Fig.14).

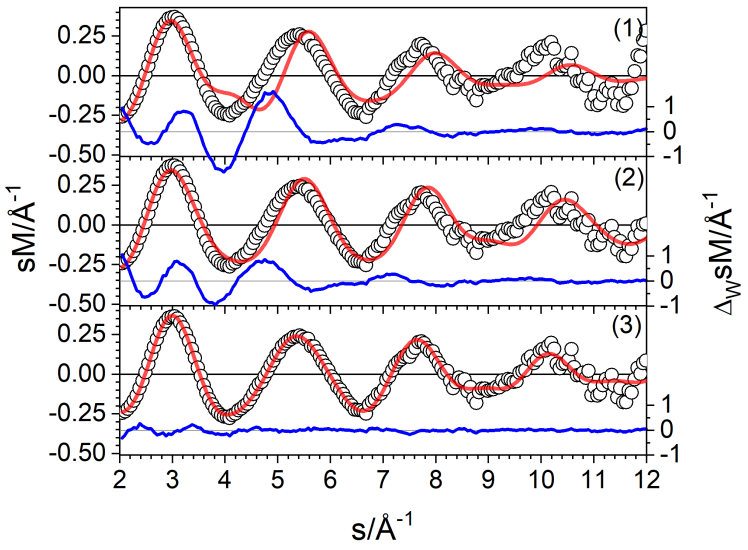

Figure 12: Comparison of experimental (grey circles) and simulated (red line) modified molecular scattering intensities sM for isomers (1)-(3) of Pt_{11}^-. The blue line in each panel shows the weighted residuals.

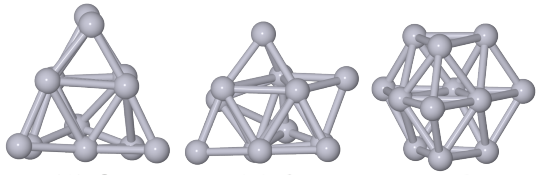

Figure 13: Pt_{12}^- isomers with point group, relative energy for TPSS/def2-TZVP, the SOC corrected value (in parentheses) and experimental profile factor.

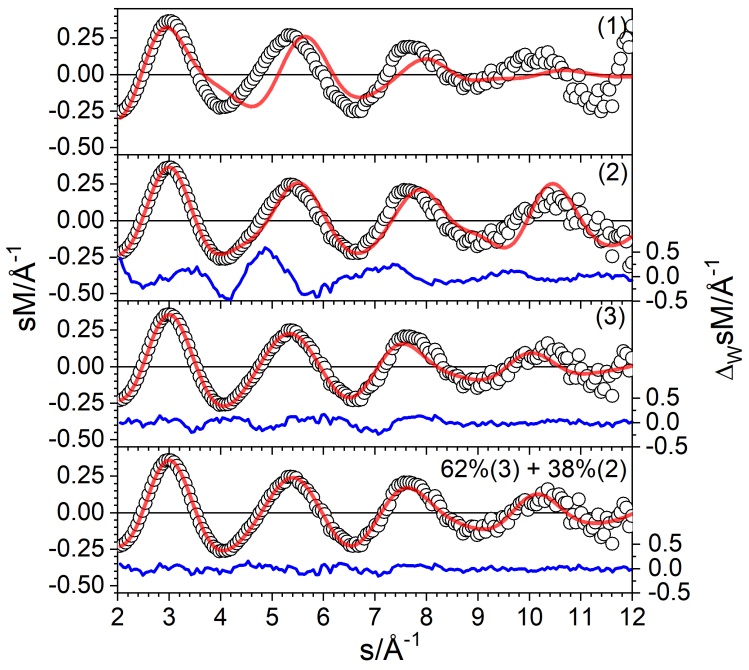

Figure 14: Comparison of experimental (grey circles) and simulated (red line) modified molecular scattering intensities sM for isomers (1)-(3) and a mixture of isomers (2) and (3) of Pt_{12}^-. The blue line in each panel shows the weighted residuals.

Pt_{13}^-

The lowest energy isomer for TPSS/def2-TZVP as well as for the 2C computations is again based on double layered trigonal structures (1) shown in Fig. 15. However, this motif can be ruled out since the simulated and experimental scattering function differ significantly. The next higher lying isomer (2) at 0.36 eV is a three capped tetrahedral structure which also shows a high profile factor. The best agreement of experiment and theory is found for isomer (3), a capped version of the truncated trigonal bipyramid (3) of Pt_{12}^-. Using TPSS/def2-TZVP it is already 0.61 eV above isomer (1), however, the relatively high energy at TPSS/def2-TZVP-level reduces significantly by inclusion of SOC (0.14 eV). The profile factor cannot be reduced by considering another isomer in a two component fit and consequently we assigned isomer (3) as the main structure for Pt_{13}^-. Typical 13-atom closed shell motifs like the icosahedron or the cuboctahedron (not shown) are even higher in energy (2.7 eV and 1.9 eV) and can also be ruled based on the TIED data (R_w = 8.2 and 10%,

respectively).

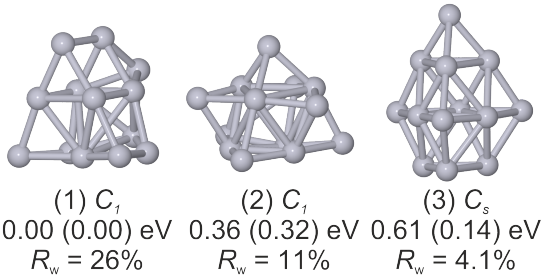

Figure 15: Pt_{13}^- isomers with point group, relative energy for TPSS/def2-TZVP, the SOC corrected value (in parentheses) and experimental profile factor.

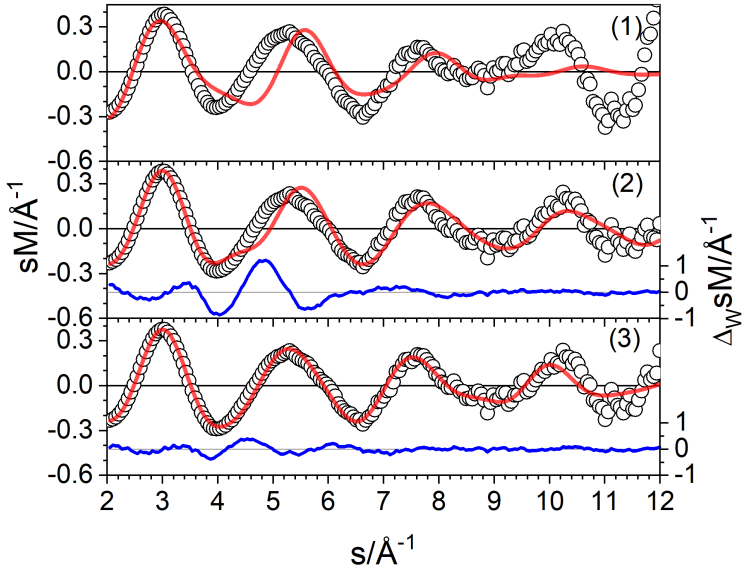

Figure 16: Comparison of experimental (grey circles) and simulated (red line) modified molecular scattering intensities sM for isomers (1)-(3) of Pt_{13}^-. The blue line in each panel shows the weighted residuals.

Discussion

Fig.17 summarizes the assigned structures for Pt_6^--Pt_{13}^-. Four different structural motifs can be identified. Pt_6^- and the major component of Pt_7^- are (quasi-) planar. The minor component of Pt_7^-, Pt_8^-, and the minor component of Pt_9^- consist of amorphous-like structures

comprised of connected trigonal and tetragonal pyramids. The major component of Pt_9^- is a defective tetrahedral structure. The tetrahedral motif then persists up to Pt_{12}^-. Finally, for Pt_{12}^- and Pt_{13}^- hcp-like structures based on trigonal bipyramids are found. Please note that at the transition sizes (Pt_7^-, Pt_9^- and Pt_{12}^-) mixtures of the neighboring motifs were found, supporting a posteriori the dual-motif ansatz. We note in passing that we cannot distinguish experimentally between a (fast) dynamic equilibrium and a static mixture of isomers.

The cluster structures were optimized using the TPSS/def2-TZVP method. The resulting structures are used to fit scattering data and the best fitting isomers are in most cases in good agreement with the experimental data. However, Pt_6^- is the only size where the TPSS/def2-TZVP global minimum agrees well with the experimental scattering data. Here, the remaining discrepancies of experimental and simulated scattering function are within the experimental error. For the larger sizes the (free) energy of the tentative global minimum and the energy of the best fitting experimental configurations differ in part significantly.

We believe that the TIED experiment probes the clusters under thermodynamic conditions. The interaction time of the clusters and the He bath gas is on the timescale of seconds; it is therefore unlikely, that the observed clusters have metastable structures. In addition, we have recently shown that, under similar experimental conditions, a chemical equilibrium is reached in the TIED experiment.[55] If we assume (thermal) equilibrium conditions here, and neglect the thermal contribution which is in the order of a few hundredths of eV (see Table S1), we can estimate the (minimal) error of the methods used. For TPSS/def2-TZVP this error is up to 0.6 eV (Pt_{12}^- and Pt_{13}^-). In addition, for Pt_9^--(4) the TPSS/def2-TZVP computation yields a qualitatively wrong result as a saddle point was predicted for the experimentally most probable structure. Inclusion of SOC by 2C-TPSS/dhf-TZVP-2c computations reduces these discrepancies to an error of 0.35 eV for Pt_8^- in this dataset. Additionally, the 2C computations correct the qualitatively incorrect TPSS/def2-TZVP result for Pt_9^--(4).

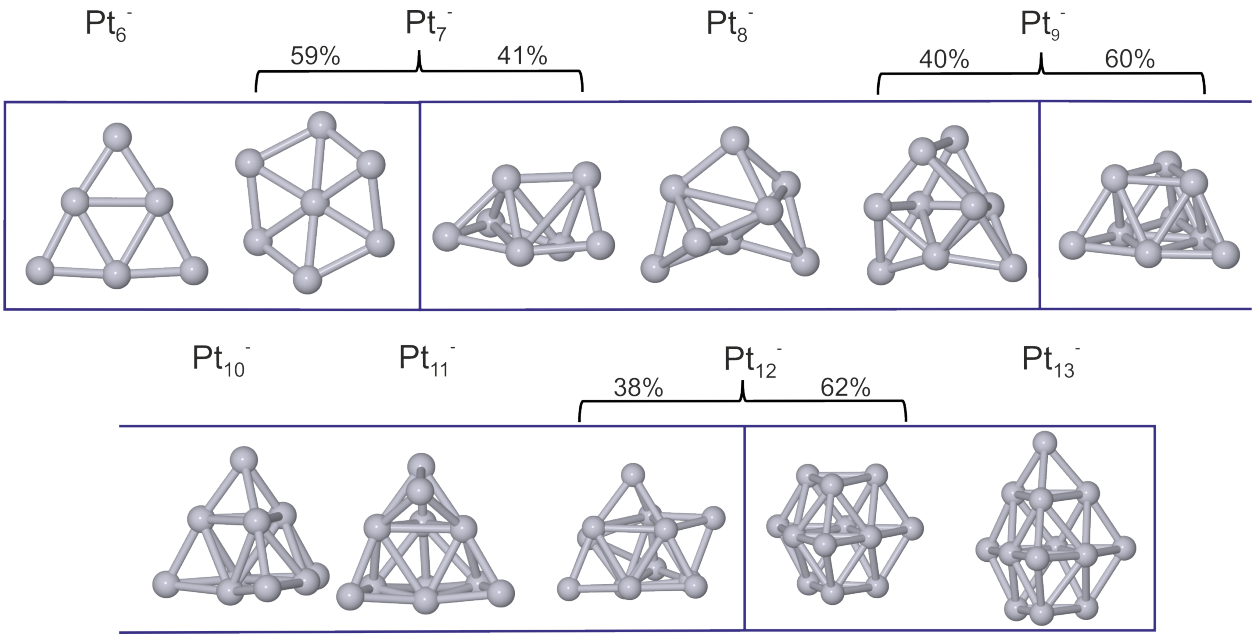

Figure 17: The assigned structures for Pt_6^--Pt_{13}^-. For Pt_7^-, Pt_9^- and Pt_{12}^- mixtures of two isomers were necessary to fit the TIED data.

Conclusion

We have studied the structures of small platinum cluster anions using a combination of trapped ion electron diffraction and density functional theory computations including spin-orbit coupling. We find that Pt_n^-, $6 \leq n \leq 13$, evolve from planar structures (Pt_6^- and Pt_7^-) via amorphous like structures (Pt_7^--Pt_9^-) and tetrahedral structures (Pt_9^--Pt_{12}^-) to structures based on an hcp motif (Pt_{12}^- and Pt_{13}^-). For most clusters, the structures found in experiment differ from the computed ground states. Spin-orbit coupling has a significant influence on the energetic ordering of isomers and reduces consistently the discrepancy between theory and experiment. Overall, we have shown that for an assessment of ground state structures TPSS/def2-TZVP is insufficient for anionic Pt clusters and even with inclusion of spin-orbit coupling a reliable assessment still requires additional reference data from experiments.

Acknowledgment

This research was supported by the German Research Foundation (Deutsche Forschungsgemeinschaft, DFG) through project 426888090 (SFB 1441) and by BMBF through the Helmholtz Association via the POF program MSE. The authors acknowledge support by the state of Baden-Württemberg through bwHPC and the German Research Foundation (DFG) through grant no INST 40/467-1 FUGG (JUSTUS cluster and bwuni cluster).

Supporting Information Available

Supporting Information is available free of charge on the ACS Publication website at DOI: containing

- Figure with two views of isomer Pt_6^--(2).
- Table with additional computational results (TPSS/dispersion, TPSS/RPA, TPSS/SOC and free energy ΔG).
- Cartesian coordinates for all isomers.

Present address: *A.G.Y: Department of Chemistry, University of Calgary, 2500 University Dr. NW, Calgary, Alberta, Canada

References

(1) Yamamoto, K.; Imaoka, T.; Chun, W.-J.; Enoki, O.; Katoh, H.; Takenaga, M.; Sonoi, A. Size-Specific Catalytic Activity of Platinum Clusters Enhances Oxygen Reduction Reactions. *Nature Chem.* **2009**, *1*, 397–402.

(2) Guo, S.; Zhang, S.; Sun, S. Tuning Nanoparticle Catalysis for the Oxygen Reduction Reaction. *Angew. Chem. Int. Ed.* **2013**, *52*, 8526–8544.

(3) Schweinberger, F. F.; Berr, M. J.; Döblinger, M.; Wolff, C.; Sanwald, K. E.; Crampton, A. S.; Ridge, C. J.; Jäckel, F.; Feldmann, J.; Tschurl, M. et al. Cluster Size Effects in the Photocatalytic Hydrogen Evolution Reaction. *J. Am. Chem. Soc.* **2013**, *135*, 13262–13265.

(4) Trevor, D. J.; Whetten, R. L.; Cox, D. M.; Kaldor, A. Gas Phase Platinum Cluster Reactions with Benzene and Several Hexanes: Evidence of Extensive Dehydrogenation and Size-Dependent Chemisorption. *J. Am. Chem. Soc.* **1985**, *107*, 518–519.

(5) Heiz, U.; Sanchez, A.; Abbet, S.; Schneider, W. D. Catalytic Oxidation of Carbon Monoxide on Monodispersed Platinum Clusters: Each Atom Counts. *J. Am. Chem. Soc.* **1999**, *121*, 3214–3217.

(6) Vajda, S.; Pellin, M. J.; Greeley, J. P.; Marshall, C. L.; Curtiss, L. A.; Ballentine, G. A.; Elam, J. W.; Catillon-Mucherie, S.; Redfern, P. C.; Mehmood, F. et al. Subnanometre Platinum Clusters as Highly Active and Selective Catalysts for the Oxidative Dehydrogenation of Propane. *Nat. Mater.* **2009**, *8*, 213–216.

(7) Imaoka, T.; Kitazawa, H.; Chun, W.-J.; Omura, S.; Albrecht, K.; Yamamoto, K. Magic Number Pt13 and Misshapen Pt12 Clusters: Which One Is the Better Catalyst? *J. Am. Chem. Soc.* **2013**, *135*, 13089–13095.

(8) Imaoka, T.; Kitazawa, H.; Chun, W.-J.; Yamamoto, K. Finding the Most Catalytically Active Platinum Clusters with Low Atomicity. *Angew. Chem. Int. Ed.* **2015**, *54*, 9810–9815.

(9) Tyo, E. C.; Vajda, S. Catalysis by Clusters with Precise Numbers of Atoms. *Nat. Nanotechnol.* **2015**, *10*, 577–588.

(10) Nesselberger, M.; Roefzaad, M.; Fayçal Hamou, R.; Ulrich Biedermann, P.; Schweinberger, F. F.; Kunz, S.; Schloegl, K.; Wiberg, G. K. H.; Ashton, S.; Heiz, U. et al. The

Effect of Particle Proximity on the Oxygen Reduction Rate of Size-Selected Platinum Clusters. *Nat. Mater.* **2013**, *12*, 919–924.

(11) Trevor, D. J.; Cox, D. M.; Kaldor, A. Methane Activation on Unsupported Platinum Clusters. *J. Am. Chem. Soc.* **1990**, *112*, 3742–3749.

(12) Harding, D. J.; Kerpal, C.; Rayner, D. M.; Fielicke, A. Communication: The Structures of Small Cationic Gas-Phase Platinum Clusters. *J. Chem. Phys.* **2012**, *136*, 211103.

(13) Henninen, T. R.; Bon, M.; Wang, F.; Passerone, D.; Erni, R. The Structure of Sub-Nm Platinum Clusters at Elevated Temperatures. *Angew. Chem. Int. Ed.* **2020**, *59*, 839–845.

(14) Xiao, L.; Wang, L. Structures of Platinum Clusters: Planar or Spherical? *J. Chem. Phys. A* **2004**, *108*, 8605–8614.

(15) Nie, A.; Wu, J.; Zhou, C.; Yao, S.; Luo, C.; Forrey, R. C.; Cheng, H. Structural Evolution of Subnano Platinum Clusters. *Int. J. Quantum Chem.* **2007**, *107*, 219–224.

(16) Kumar, V.; Kawazoe, Y. Evolution of Atomic and Electronic Structure of Pt Clusters: Planar, Layered, Pyramidal, Cage, Cubic, and Octahedral Growth. *Phys. Rev. B* **2008**, *77*, 205418.

(17) Fung, V.; Jiang, D.-e. Exploring Structural Diversity and Fluxionality of Ptn (N = 10–13) Clusters from First-Principles. *J. Phys. Chem. C* **2017**, *121*, 10796–10802.

(18) Demiroglu, I.; Yao, K.; Hussein, H. A.; Johnston, R. L. Dft Global Optimization of Gas-Phase Subnanometer Ru–Pt Clusters. *J. Phys. Chem. C* **2017**, *121*, 10773–10780.

(19) Li, R.; Odunlami, M.; Carbonnière, P. Low-Lying Ptn Cluster Structures (N=6–10) from Global Optimizations Based on Dft Potential Energy Surfaces: Sensitivity of the Chemical Ordering with the Functional. *Comput. Theor. Chem.* **2017**, *1107*, 136–141.

(20) Chaves, A. S.; Piotrowski, M. J.; Da Silva, J. L. F. Evolution of the structural, energetic, and electronic properties of the 3d, 4d, and 5d transition-metal clusters (30 TMn systems for n = 2–15): a density functional theory investigation. *Phys. Chem. Chem. Phys.* **2017**, *19*, 15484–15502.

(21) Weis, P. Structure Determination of Gaseous Metal and Semi-Metal Cluster Ions by Ion Mobility Spectrometry. *Int. J. Mass Spectrom.* **2005**, *245*, 1–13.

(22) Schooss, D.; Weis, P.; Hampe, O.; Kappes, M. M. Determining the Size-Dependent Structure of Ligand-Free Gold-Cluster Ions. *Philos. Trans. R. Soc. London, A* **2010**, *368*, 1211–1243.

(23) Chaves, A. S.; Rondina, G. G.; Piotrowski, M. J.; Tereshchuk, P.; Da Silva, J. L. F. The Role of Charge States in the Atomic Structure of Cun and Ptn (N = 2–14 Atoms) Clusters: A Dft Investigation. *J. Chem. Phys. A* **2014**, *118*, 10813–10821.

(24) Zhai, H.; Alexandrova, A. N. Fluxionality of Catalytic Clusters: When It Matters and How to Address It. *ACS Catal.* **2017**, *7*, 1905–1911.

(25) Häkkinen, H.; Abbet, W.; Sanchez, A.; Heiz, U.; Landman, U. Structural, Electronic, and Impurity-Doping Effects in Nanoscale Chemistry: Supported Gold Nanoclusters. *Angew. Chem. Int. Ed.* **2003**, *42*, 1297–1300.

(26) Johansson, M. P.; Lechtken, A.; Schooss, D.; Kappes, M. M.; Furche, F. 2d-3d Transition of Gold Cluster Anions Resolved. *Phys. Rev. A* **2008**, *77*, 053202–053207.

(27) Kelting, R.; Baldes, A.; Schwarz, U.; Rapps, T.; Schooss, D.; Weis, P.; Neiss, C.; Weigend, F.; Kappes, M. M. Structures of Small Bismuth Cluster Cations. *J. Chem. Phys.* **2012**, *136*, 154309–154301–154310.

(28) Huda, M. N.; Niranjan, M. K.; Sahu, B. R.; Kleinman, L. Effect of Spin-Orbit Coupling on Small Platinum Nanoclusters. *Phys. Rev. A* **2006**, *73*, 053201.

(29) Sebetci, A. Does Spin–Orbit Coupling Effect Favor Planar Structures for Small Platinum Clusters? *Phys. Chem. Chem. Phys.* **2009**, *11*, 921–925.

(30) Nair, A. S.; Anoop, A.; Ahuja, R.; Pathak, B. Relativistic Effects in Platinum Nanocluster Catalysis: A Statistical Ensemble-Based Analysis. *J. Chem. Phys. A* **2022**, *126*, 1345–1359.

(31) Schooss, D.; Kappes, M. M. In *Encyclopedia of Interfacial Chemistry*; Wandelt, K., Ed.; Elsevier: Oxford, 2018; pp 567–579.

(32) Kraft, M.; Flores, J. R.; Klopper, W.; Kappes, M. M.; Schooss, D. Structures of Small Tantalum Cluster Anions: Experiment and Theory. *J. Phys. Chem. A* **2021**, *125*, 3135–3145.

(33) Waldt, E.; Hehn, A.-S.; Ahlrichs, R.; Kappes, M. M.; Schooss, D. Structural Evolution of Small Ruthenium Cluster Anions. *J. Chem. Phys.* **2015**, *142*, 024319.

(34) Schooss, D.; Blom, M. N.; Parks, J. H.; Issendorff, B. v.; Haberland, H.; Kappes, M. M. The Structures of Ag55+ and Ag55-: Trapped Ion Electron Diffraction and Density Functional Theory. *Nano Lett.* **2005**, *5*, 1972–1977.

(35) Haberland, H.; Mall, M.; Moseler, M.; Qiang, Y.; Reiners, T.; Thurner, Y. Filling of Micron-Sized Contact Holes with Copper by Energetic Cluster Impact. *J. Vac. Sci. Technol., A* **1994**, *12*, 2925–2930.

(36) Wilson, A. J. C.; Prince, E. In *Internaltional tables of crystallography*; Doordrecht/Boston/London, Ed.; Kluwer Academic Publishers, 1999.

(37) Gupta, R. P. Lattice Relaxation at a Metal Surface. *Phys. Rev. B* **1981**, *23*, 6265–6270.

(38) Cleri, F.; Rosato, V. Tight-binding potentials for transition metals and alloys. *Phys. Rev. B* **1993**, *48*, 22–33.

(39) Doye, J. P. K.; Wales, D. J.; Berry, R. S. The effect of the range of the potential on the structures of clusters. *J. Chem. Phys.* **1995**, *103*, 4234–4249.

(40) Neiss, C.; Schooss, D. Accelerated Cluster Structure Search Using Electron Diffraction Data in a Genetic Algorithm. *Chem. Phys. Lett.* **2012**, *532*, 119–123.

(41) Rapps, T.; Ahlrichs, R.; Waldt, E.; Kappes, M. M.; Schooss, D. On the Structures of 55-Atom Transition-Metal Clusters and Their Relationship to the Crystalline Bulk. *Angew. Chem. Int. Ed.* **2013**, *52*, 6102–6105.

(42) TURBOMOLE V7.2 2017, a development of University of Karlsruhe and Forschungszentrum Karlsruhe GmbH, 1989-2007, TURBOMOLE GmbH, since 2007; available from http://www.turbomole.com.

(43) Sierka, M. Synergy between Theory and Experiment in Structure Resolution of Low-Dimensional Oxides. *Prog. Surf. Sci.* **2010**, *85*, 398–434.

(44) Weigend, F.; Ahlrichs, R. Balanced Basis Sets of Split Valence, Triple Zeta Valence and Quadruple Zeta Valence Quality for H to Rn: Design and Assessment of Accuracy. *Phys. Chem. Chem. Phys.* **2005**, *7*, 3297–3305.

(45) Becke, A. D. Density-Functional Exchange-Energy Approximation with Correct Asymptotic Behavior. *Phys. Rev. A* **1988**, *38*, 3098–3100.

(46) Eichkorn, K.; Treutler, O.; Öhm, H.; Häser, M.; Ahlrichs, R. Auxiliary Basis Sets to Approximate Coulomb Potentials. *Chem. Phys. Lett.* **1995**, *240*, 283–290.

(47) Eichkorn, K.; Weigend, F.; Treutler, O.; Ahlrichs, R. Auxiliary Basis Sets for Main Row Atoms and Transition Metals and Their Use to Approximate Coulomb Potentials. *Theor. Chem. Acc.* **1997**, *97*, 119–124.

(48) Andrae, D.; Häußermann, U.; Dolg, M.; Stoll, H.; Preuß, H. Energy-Adjusted ab initio

Pseudopotentials for the Second and Third Row Transition Elements. *Theor. Chim. Acta* **1990**, *77*, 123–141.

(49) Tao, J.; Perdew, J. P.; Staroverov, V. N.; Scuseria, G. E. Climbing the Density Functional Ladder: Nonempirical Meta–Generalized Gradient Approximation Designed for Molecules and Solids. *Phys. Rev. Lett.* **2003**, *91*, 146401.

(50) Lechtken, A.; Neiss, C.; Kappes, M. M.; Schooss, D. Structure Determination of Gold Clusters by Trapped Ion Electron Diffraction: Au_{14}^- - Au_{19}^-. *Phys. Chem. Chem. Phys.* **2009**, *11*, 4344–4350.

(51) Armbruster, M. K.; Weigend, F.; van Wüllen, C.; Klopper, W. Self-Consistent Treatment of Spin–Orbit Interactions with Efficient Hartree–Fock and Density Functional Methods. *Phys. Chem. Chem. Phys.* **2008**, *10*, 1748–1756.

(52) Weigend, F.; Baldes, A. Segmented Contracted Basis Sets for One- and Two-Component Dirac–Fock Effective Core Potentials. *J. Chem. Phys.* **2010**, *133*, 174102.

(53) Figgen, D.; Peterson, K. A.; Dolg, M.; Stoll, H. Energy-Consistent Pseudopotentials and Correlation Consistent Basis Sets for the 5d Elements Hf–Pt. *J. Chem. Phys.* **2009**, *130*, 164108.

(54) Grimme, S.; Ehrlich, S.; Goerigk, L. Effect of the Damping Function in Dispersion Corrected Density Functional Theory. *J. Comput. Chem.* **2011**, *32*, 1456–1465.

(55) Hehn, A.-S.; Bumüller, D.; Klopper, W.; Kappes, M. M.; Schooss, D. Structural Phase Transition of Ruthenium Cluster Hydrides. *J. Phys. Chem. C* **2020**, *124*, 14306–14315.

TOC Graphic